1978

A Comparison of SRM and Globoid Type Screw Compressors at Full Load

A. Lundberg

R. Glanvall

A COMPARISON OF SRM AND GLOBOID TYPE SCREW COMPRESSORS AT FULL LOAD

Anders Lundberg, Chief Engineer
Rune Glanvall, Compressor Projects Engineer
STAL Refrigeration AB, Norrköping, Sweden

INTRODUCTION

Different types of compressors can be compared in different ways. Comparisons can be based on capacity/compactness ratio, operating range, etc. The method selected will depend on the purpose of the comparison.

In this paper two positive deplacement compressors will be compared. Both are screw compressors of the oil-injected, capacity-controlled type. Conventional screw compressors of the SRM type (Fig. 1S) will be compared with the Globoid type compressors (Fig. 1G).

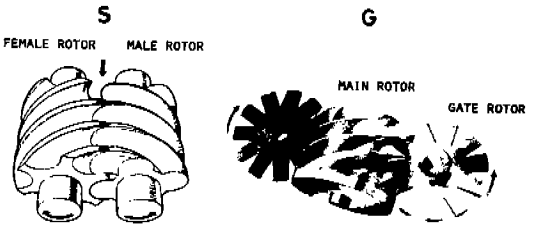

Fig. 1 SRM (S) and Globoid (G) type screw compressors

The comparison will be based primarily on the efficiencies of the two types of compressors.
First each compressor's geometry, volume curves, volume change rates, port areas, pressure drops, leakage areas, theoretical ratios of part load, etc. will be analyzed theoretically. The results of this theoretical analysis will then be compared with data obtained from test runs conducted using two compressors having the same swept volume – about 1250 m^3/h at 3000 rpm. Both compressors are available on the market and are of normal production quality.

The tests were run using NH_3 and R22, and the same test rigs were used for both compressors.
Moreover, the operating conditions were the same. Both compressors were tested at full load and also at part load and with different built-in volume ratios, one low and one high, and at different condensing temperatures (discharge pressures) evaporation temperatures (suction pressures), speed, etc. The amounts of oil that were injected were optimized for each built-in volume ratio. The individual manufacturer's instructions were followed in all other respects.

The compressors were driven and the compressor input torque was measured by a DC dynamometer motor. The gas flow rate was measured with nozzles at the compressor suction side in accordance with ISO 917 - 1974 and ISO R541. The R22 refrigerant data were taken from "Thermodynamic Properties of Freon 22 (T22) " (Du Pont de Nemours and Company) and the NH_3 data were taken from "ASHRAE Guide and Data Book, 1965"

The tests were run under the supervision of an official inspector from The Aeronautical Research Institute of Sweden.

The isentropic efficiency was selected as the basis for comparison. Isentropic efficiency is defined as

$$\eta_{is} = \frac{\dot{m} \cdot \Delta h_{is}}{P} \qquad \ldots\ldots\ldots\ldots\ldots 1$$

where $\dot{m}$ = measured mass flow

Δh_{is} = isentropic enthalpy difference at constant entropy

P = power input to the compressor

This paper is divided in two parts. The first presents the theoretical analysis and test results for full load, while the second presents corresponding information for part load.

CONFIGURATION

The SRM compressor (Fig.1S) consists, in principle, of two meshing helical rotors. These rotors are provided with a special asymmetric lobe-profile. A 4-lobe male rotor is used in combination with a 6-lobe female rotor. Inflow into the interlobe space is normally axial at one end plane. The gas moves axially during compression toward the other end plane where it discharges through radial and axial outlet ports. The swept volume is defined as

$$V_S = (A_M + A_F) \cdot L \cdot Z \cdot C \qquad rev^{-1} \ldots\ldots\ldots\ldots\ldots 2$$

where A_M, A_F = cross-sectional areas as per Fig. 2.

L = rotor length

Z = number of lobes on driving rotor

C = constant that depends on rotor profile and wrap angle

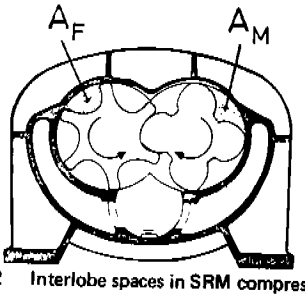

Fig. 2 Interlobe spaces in SRM compressors

The compressor swept volume can be varied by varying the rotor diameter and/or rotor length and also by driving either the male rotor or female rotor.

The Globoid compressor consists of a globoid screw and two gate rotors which comprise the rotating sealing elements. Both the main rotor and the gate rotors can vary within wide limits with regard to form and mutual geometry. The normally encountered designs are shown in principle in Fig. 1G. The main rotor has six entrances for the 11 teeth on each of the gate rotors. Fig. 3 illustrates the geometry and shows how the swept volume V_G is calculated.

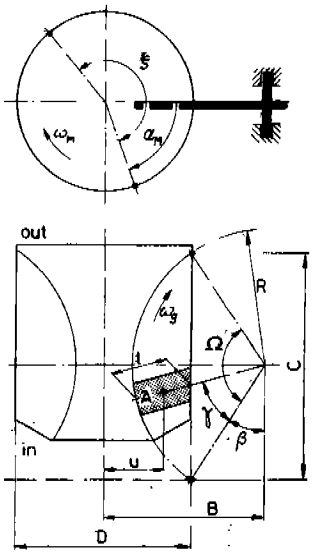

Fixed parameters

Main Rotor Diam.	D
Gate Rotor Radius	R
Gate Rotor Centre	B
Wrap Angle	ξ
Angular Speed	ω

Formulas

$\beta = \arcsin \frac{B-D/2}{R}$ (const.)

$\Omega = \pi - 2\beta$ (const.)

$C = 2 \cdot R \cdot \sin \frac{\Omega}{2}$ (const.)

$\gamma = \alpha \frac{\Omega}{\xi}$

$t = R - \frac{B-D/2}{\sin(\beta+\gamma)}$

$u = B - D/2 + t/2 \cdot \sin(\beta+\gamma)$

$V_G = \sum_{\alpha=\alpha_i}^{\xi} A \cdot u \cdot \Delta\alpha$

Fig. 3 Geometry of Globoid compressors

The normally encountered designs have either an axial or radial inlet. The gas is moved axially via the main rotor groove and discharges through a radial outlet port. The compressor that was tested has an axial inlet.

If the rotor dimensions are fixed relative to the main rotor diameter, the swept volume is

$$V_G = f\,(D^3) \quad \ldots\ldots\ldots\ldots\ldots\ldots\ldots\ldots 3$$

Only the main rotor can be driven.

COMPRESSOR OPERATING PRINCIPLES

Both types of compressors are positive displacement compressors. Neither had working valves and both had a built-in volume ratio, v_i.

The working cycles of the individual compressors are illustrated by the volume curves in Fig. 4. Here, the left-hand ascending part of the curve represents the suction cycle while the descending part at right represents the compression and discharge cycles. The built-in volume ratio v_i is a geometric definition obtained as follows

$$v_i = \frac{V_S}{V_i} \text{ or } \frac{V_G}{V_i} \quad \ldots\ldots\ldots\ldots\ldots\ldots\ldots\ldots 4$$

where V_S or V_G = theoretical interlobe space volume when inlet closes

V_i = theoretical interlobe space volume when outlet opens

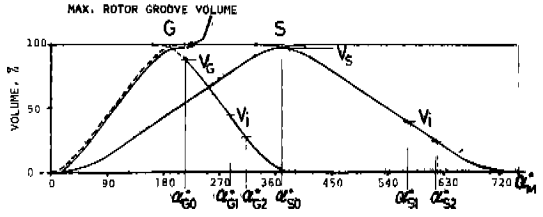

Fig. 4 Volume curves for SRM and Globoid compressors

The overlapping of the suction and compression parts of the individual curves is attributable to the wrap angle, and this affects the swept volume (constant C in the formula 2). The positions of the outlet ports are determined by the desired v_i. At full load, the compressor efficiency is heavily influenced by v_i, due to the fact that the compressor geometry is optimized for full load operation.

The operating conditions determine which v_i should be selected. This is accomplished using the following

$$v^n = \frac{P1}{P2} \quad \ldots\ldots\ldots\ldots\ldots\ldots\ldots\ldots 5$$

where P1 = discharge pressure

P2 = suction pressure

n = polytropic exponent of the compression process

The Globoid compressor is symmetric relative to the rotor casing partition. This means that the working cycle is run through faster, as shown in Fig. 4.

Figures 5 and 6 present diagrammatic developments of the rotors used in the SRM and Globoid compressor respectively, as well as the shapes and positions of the outlet ports for two values of v_i, one low and one high.

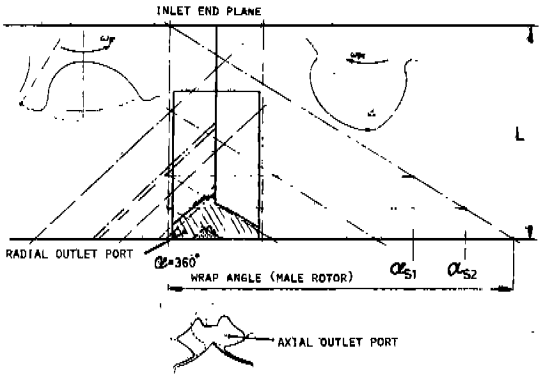

Fig. 5 Diagrammatic development of rotor surfaces and outlet ports in the SRM compressor

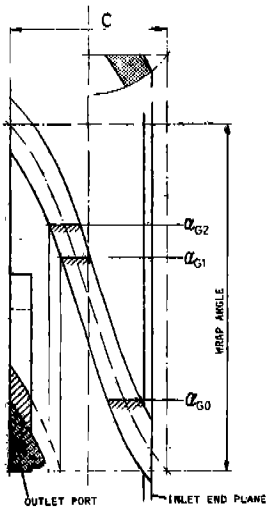

Fig. 6 Diagrammatic development of rotor surface (one groove) and outlet ports in the Globoid compressor

ANALYSIS OF LOSSES

Volume Change – Gas Velocity – Pressure Drop

The volume curve, the compressor geometry (rotorprofile and the shapes, positions and areas of the inlet and outlet ports), the volume change per unit of time and the gas velocities are calculated on the basis of the swept volume and the compressor dimensions. Fig. 7 illustrates the inlet conditions for the two analyzed compressors. The fast volume change (ΔV) in the SRM compressor is counteracted by the considerably larger inlet areas (A) to the interlobe spaces. This results in a lower inflow velocity as compared with the conditions that prevail in the Globoid compressor. Fig. 8 shows the individual inflow velocities as a function of the theoretical interlobe space volume.

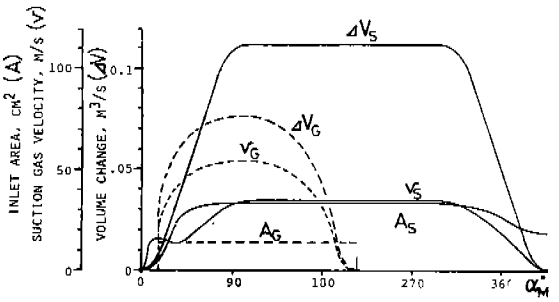

Fig. 7 Inlet conditions for the SRM (S) and the Globoid (G) compressors

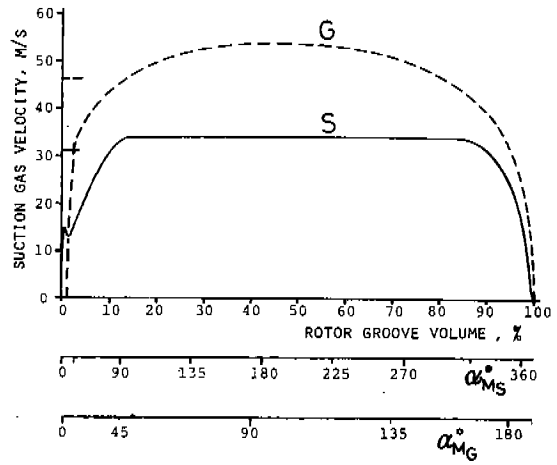

Fig. 8 Inflow velocity during the suction cycle for the SRM and the Globoid compressors

The conditions that prevail during the outlet cycle are shown in Fig. 9 for the SRM compressor and Fig. 10 for the Globoid compressor at two different values of v_i. Figures 5 and 6 show that the increase in v_i causes a decrease in the outlet areas. This is also indicated in Figures 9 and 10 where the gas velocity through the outlet ports is higher for the high v_i as long as the actual flow area is determined by the configuration of the outlet ports. Fig. 11 shows the outflow velocity as a function of the theoretical interlobe space volume.

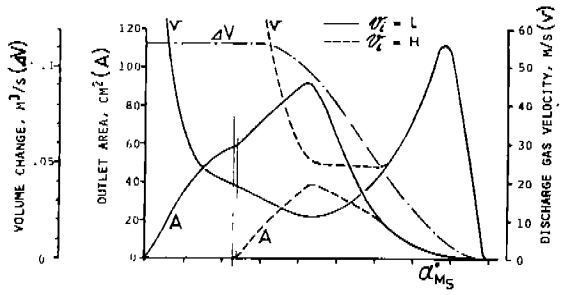

Fig. 9 Outlet conditions for the SRM compressor

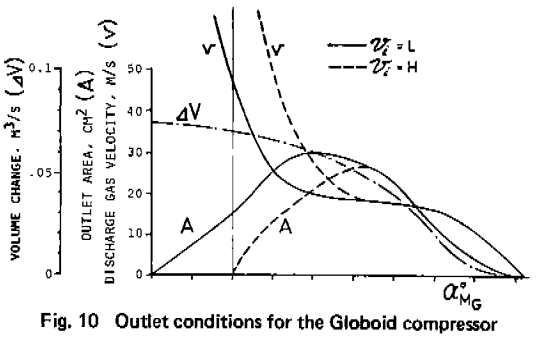

Fig. 10 Outlet conditions for the Globoid compressor

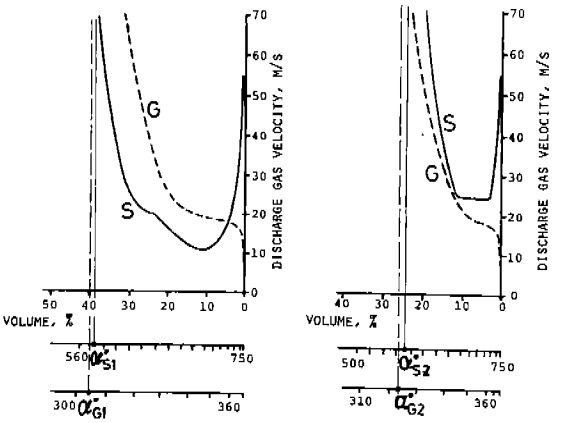

Fig. 11 Discharge gas velocity during the outlet cycle for the SRM and the Globoid compressors

The instantaneous pressure drop (Δp) is calculated from the diagrams shown in Figures 8 and 11 using the following

$$\Delta p = \rho \cdot \xi \cdot \frac{V^2}{2} \quad N/m^2 \qquad \ldots\ldots\ldots\ldots\ldots\ldots\ldots\ldots 6$$

where

ρ = density, kg/m³

ξ = coefficient of resistance for the flow area

V = flow velocity, m/s

PV diagram

From a PV diagram for a compressor operating at v_i, one can analyze different losses – inlet pressure drop loss, outlet pressure drop loss, and the v_i loss. The v_i loss is the loss caused by work attributable to the fact that $P_1/P_2 \neq v_i^n$ (Figures 12 and 13). Moreover, the actual compressor cycle can be read from a PV diagram plotted from measured data.

Fig. 12 shows a schematic, polytropic compressor cycle.

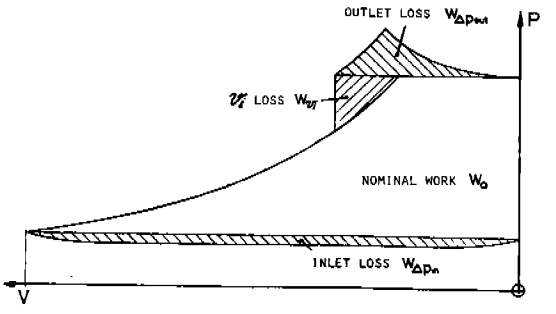

Fig. 12 Schematic PV diagram

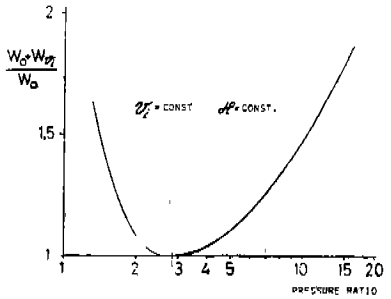

Fig. 13 Variation in v_i loss with pressure ratio

As mentioned previously, tests were made using R22 and ammonia (NH_3) as refrigerants.

The polytropic exponents for these refrigerants in the types of compressors tested were taken from experimental data. This also applies to ρ and ξ for the operating conditions and compressors in question. On the basis of these values, the pressure drop and v_i losses have been calculated, and Fig. 14 shows a theoretical PV diagram for an approximately optimal operating situation.

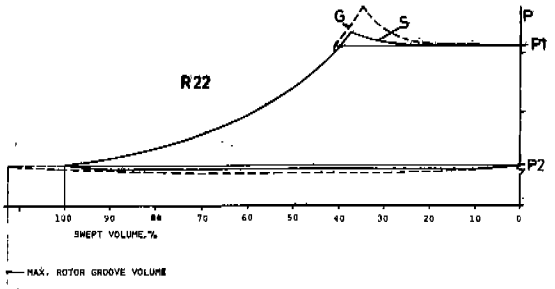

Fig. 14 Theoretic PV diagram for the SRM and the Globoid compressors for a certain situation

Fig. 15 shows the calculated partial and total losses attributable to the pressure drop in the inlet and outlet areas for $P1/P_2 = v^n$. Surprisingly, the inlet losses are high, and, in certain cases, close to twice Δp_{out} for heavy refrigerants. It is also evident that the relatively small areas in the Globoid compressor provide greater pressure drop losses than those sustained in the SRM compressor, which nonetheless has an unfavourable outlet area for high values of v_i.

		v_i = LOW			v_i = HIGH		
COMPR. TYPE	REFR.	$\frac{W\Delta p_{in}}{W_o}$	$\frac{W\Delta p_{out}}{W_o}$	$\frac{W_o+W\Delta p}{W_o}$	$\frac{W\Delta p_{in}}{W_o}$	$\frac{W\Delta p_{out}}{W_o}$	$\frac{W_o+W\Delta p}{W_o}$
S	NH_3	0.004	0.003	1.007	0.003	0.006	1.009
	R22	0.024	0.016	1.040	0.016	0.036	1.052
G	NH_3	0.011	0.010	1.021	0.007	0.005	1.012
	R22	0.062	0.060	1.122	0.044	0.026	1.070

Fig. 15 Pressure drop losses in the inlet and outlet areas

Leakage Losses

Both the SRM and Globoid compressors have leakage areas between sequential interlobe spaces and also directly between the outlet and inlet sides.

Blow holes are encountered in both compressors. In the SRM compressor they are between the interlobe spaces, and in the Globoid compressor they are directly between the rotor groove and the inlet.

Fig. 16 shows the leakage paths in the SRM compressor. The paths shown in Fig. 16a are in the outlet plane and above the rotor lobes. In Fig. 16b these paths proceed via the mesh line and in Fig. 16c they consist of the aforesaid blow holes.

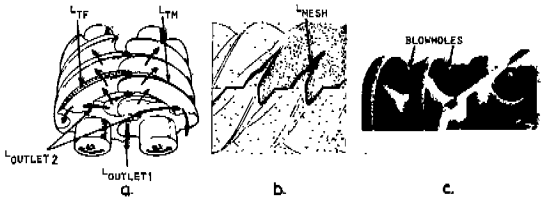

Fig. 16 Leakage paths and blow holes in the SRM compressor

Fig. 17 shows, in diagram form, the leakage line lengths in the SRM compressor per interlobe space. Fig. 18 shows the total instantaneous sealing line length and its mean value for a single rotor revolution.

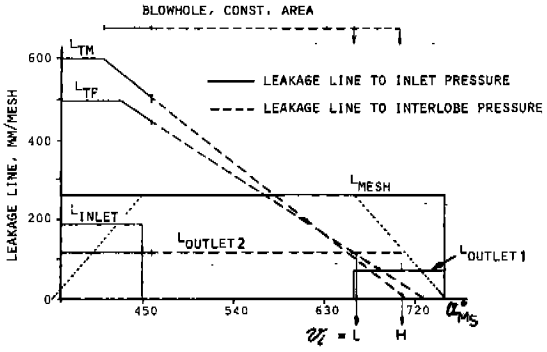

Fig. 17 Variation in length of leakage paths per interlobe space in the SRM compressor

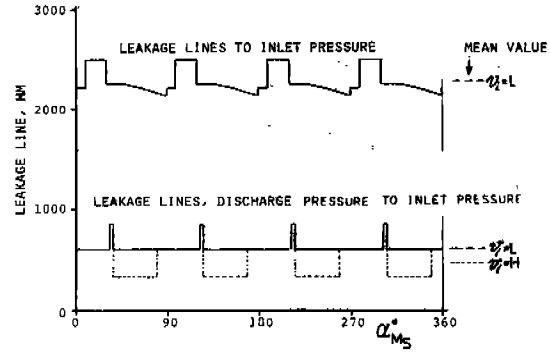

Fig. 18 Total length of leakage paths and mean length for one male rotor revolution in the SRM compressor

Figures 19, 20 and 21 present the corresponding information for the Globoid compressor.

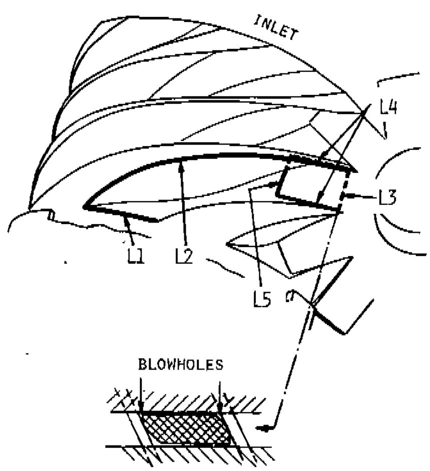

Fig. 19 Leakage paths and blow holes in the Globoid compressor

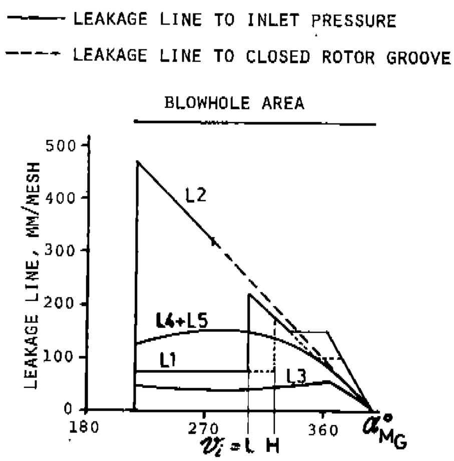

Fig. 20 Variation in length of leakage paths per rotor groove in the Globoid compressor

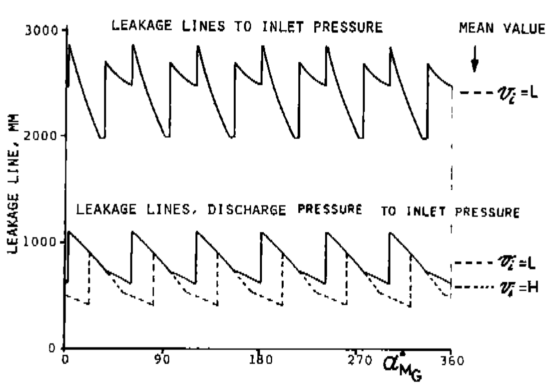

Fig. 21 Total length of leakage paths and mean length for one main rotor revolution in the Globoid compressor

Leakage to an interlobe space volume that is closed on the inlet side affects power consumption, while leakage to the inlet side with open inlet port affects both power consumption and volumetric efficiency (η_v).

The amount of leakage depends on the leakage area and the difference in pressure. The following applies for leakage from the high-pressure side directly to the inlet

$$\frac{\eta_v}{\eta_{is}} = \text{constant} \qquad (7)$$

That is to say, a change in η_v provides a proportional change in η_{is}. For leakage from pressure levels lower than the maximum pressure to the inlet side, a different relationship applies since the compression work is decreased and this causes a change in n (polytropic exponent). See Fig. 22.

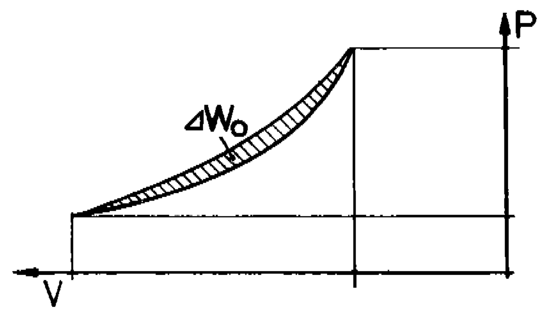

Fig. 22 Decreasing compression work due to leakage from intermediate pressure levels to the inlet side

A comparison of Figures 18 and 21 shows that the Globoid compressor has a total leakage line length(adjusted to the same swept volume)towards the inlet which is approximately 13% longer than in the SRM compressor. The leakage line, not including blow holes, between the outlet pressure and the inlet is approximately 46% longer in the Globoid compressor for a low value of v_i and approximately 37% longer for a high value of v_i .

Other Losses

The compressors that were tested are of approximately the same size. Consequently, other losses such as ventilation and friction losses are of the same order of magnitude. The main rotor in the Globoid compressor is, in principle, unloaded both axially and radially with regard to forces exerted by the gas, but a small torque is transmitted to the gate rotors, and their bearings are exposed to both radial and axial forces. The friction losses in the bearings are small and are considered equal in the two types of compressors due to the fact that there are six bearings in both types.

Summary of Theoretical Loss Analysis

The theoretical loss analysis indicates that pressure drop losses are greater in the Globoid compressor than in the SRM compressor and this entails greater power consumption. The leakage losses are also higher in the Globoid compressor, but because of a difference in the relationship between leakage directly to the inlet and leakage to the "closed volumes" it is expected that the Globoid compressor will have considerably lower volumetric efficiency than the SRM compressor. Moreover, this difference is expected to increase as the pressure ratio increases. When NH_3 is used, both the total and relative volumetric efficiencies should be less than when R22 is used. However, at a low pressure ratio and particularly when R22 is used, the Globoid compressor can provide a better η_v than the SRM compressor.

Even though it may seem contradictory, a study of the volume curve in Fig. 4 shows that the Globoid compressor can be considered as "supercharged". It becomes evident that the maximum rotor groove volume is greater than V_G and that this depends on the design. This means that η_v, which is calculated on the basis of V_G, could be close to 100%, theoretically even higher.

Because of the long direct leakage line towards the inlet, η_v is affected more extensively in the Globoid compressor than in the SRM compressor, but because of the aforesaid longer leakage line between intermediate pressure levels and the inlet side the total efficiency is not affected proportionally with changes in η_v.

As mentioned previously, the other losses are equivalent for the two types of compressors and do not have any effect on their relative performance.

TEST RESULTS AT FULL LOAD

It is only possible to present a selected portion of the test results in this paper because of space considerations. Figures 23 and 24 show the full-load efficiencies and the specific torque applied for low and high values of v_i using ammonia at constant condensing pressure. Figures 25 and 26 show the corresponding results for R22 as per the previously described test method.

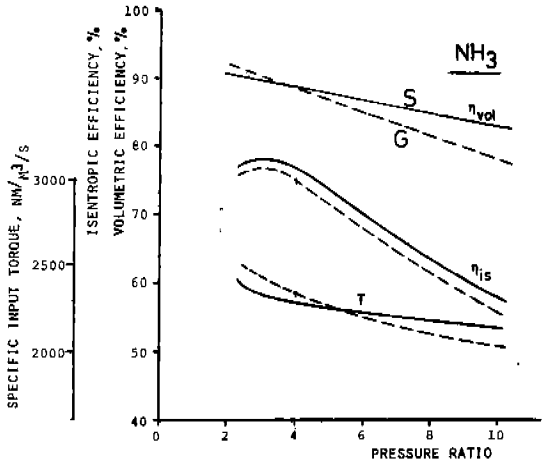

Fig. 23 Ammonia compressor efficiencies for the SRM and the Globoid compressors at low v_i

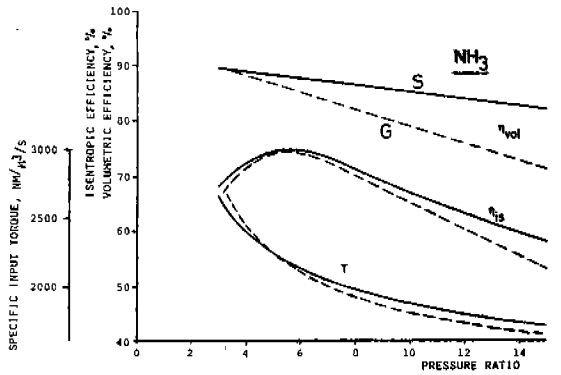

Fig. 24 Ammonia compressor efficiencies for the SRM and the Globoid compressors at high v_i

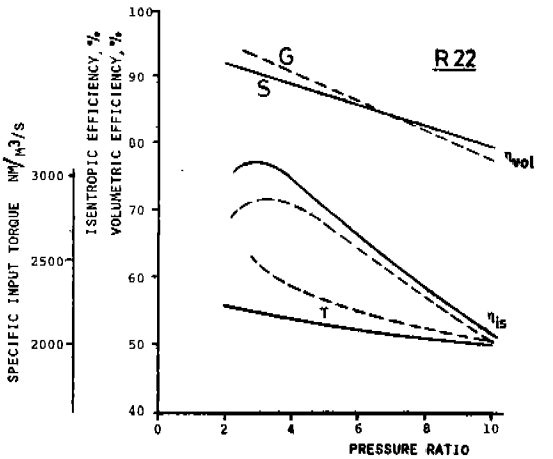

Fig. 25 R22 compressor efficiencies for the SRM and the Globoid compressors at low v_i

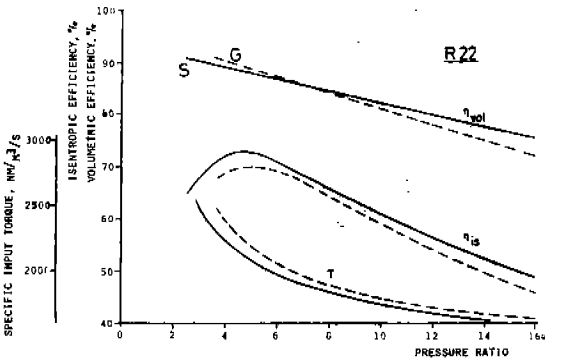

Fig. 26 R22 compressor efficiencies for the SRM and the Globoid compressors at high v_i

The test results show that the effects predicted by the theoretical loss analysis did occur. The Globoid compressor had a somewhat better η_v than the SRM compressor at a low pressure ratio, particularly for R22. However, the η_v curve dropped more steeply when approaching a high P1/P2. The torque curve T also showed that the calculated effects of flow losses and leakage agreed very well with the actual conditions encountered, particularly with regard to the differences between the two refrigerants.

A comparison between the theoretical and actual results shows that a careful theoretical analysis of the two types of compressors provides an accurate picture of the sources of loss, their inter-relationships and their causes. It also shows that it is possible at an early stage to estimate the effects of changes. Moreover, it indicates that new techniques and new products can be evaluated relative to existing techniques and products.

This paper, which has discussed the design, operation and full-load conditions for the SRM and Globoid types of screw compressors is the first part of a 2-part analysis.
The second part presents part-load conditions and the results of the part-load tests.